New Phytologist

Research

Optimal carbon partitioning helps reconcile the apparent divergence between optimal and observed canopy profiles of photosynthetic capacity

Thomas N. Buckley[1]

[1]Department of Plant Sciences, University of California, Davis, One Shields Ave, Davis, CA 95616, USA

Author for correspondence:
Thomas N. Buckley
Email: tnbuckley@ucdavis.edu

Received: *31 October 2020*
Accepted: *7 January 2021*

New Phytologist (2021)
doi: 10.1111/nph.17199

Key words: canopies, optimality, photosynthesis, stomata, transpiration.

Summary

- Photosynthetic capacity per unit irradiance is greater, and the marginal carbon revenue of water ($\partial A/\partial E$) is smaller, in shaded leaves than sunlit leaves, apparently contradicting optimization theory. I tested the hypothesis that these patterns arise from optimal carbon partitioning subject to biophysical constraints on leaf water potential.
- In a whole plant model with two canopy modules, I adjusted carbon partitioning, nitrogen partitioning and leaf water potential to maximize carbon profit or canopy photosynthesis, and recorded how gas exchange parameters compared between shaded and sunlit modules in the optimum.
- The model predicted that photosynthetic capacity per unit irradiance should be larger, and $\partial A/\partial E$ smaller, in shaded modules compared to sunlit modules. This was attributable partly to radiation-driven differences in evaporative demand, and partly to differences in hydraulic conductance arising from the need to balance marginal returns on stem carbon investment between modules. The model verified, however, that invariance in the marginal carbon revenue of N ($\partial A/\partial N$) is in fact optimal.
- The Cowan–Farquhar optimality solution (invariance of $\partial A/\partial E$) does not apply to spatial variation within a canopy. The resulting variation in carbon–water economy explains differences in capacity per unit irradiance, reconciling optimization theory with observations.

Introduction

Scaling photosynthesis and transpiration from leaves to canopies is made difficult by wide spatial variation among canopy locations in key parameters that determine gas exchange, particularly photosynthetic capacity and stomatal conductance. Modelers commonly use optimization theory – the hypothesis that plants have evolved to maximize the return on investment of limiting resources – to infer canopy profiles of gas exchange parameters (Amthor, 1994; de Pury & Farquhar, 1997). Applied to canopy photosynthesis, optimization theory predicts that a fixed total supply of photosynthetic nitrogen (N) is optimally distributed when the marginal carbon product of N, $\partial A/\partial N$, is invariant among canopy positions and among functional N pools within each location (Field, 1983):

$$\frac{\partial A}{\partial N}(\mathbf{p},\mathbf{x}) = \mu_n \qquad \text{Eqn 1}$$

where A is net CO_2 assimilation rate, averaged over some period, such as 1 d, during which it is assumed that N cannot be redistributed among pools or locations ($\mathbf{p}$ and $\mathbf{x}$ denote vectors of functional N pools (carboxylation, regeneration and light harvesting) and canopy positions, respectively; and μ_n is a Lagrange multiplier that is invariant among N pools and canopy positions; a list of symbols is given in Table 1). When Eqn 1 is applied to simple models of canopy gas exchange, it predicts that photosynthetic capacity should vary among canopy locations in proportion to the average daily or seasonal irradiance (Field, 1983; Hirose & Werger, 1987; Farquhar, 1989; Sands, 1995), or equivalently, that the ratio of photosynthetic capacity between any two canopy layers should be equal to the ratio of irradiance between the layers. That prediction is very useful for upscaling models of leaf photosynthesis, because it allows an unknown biological property (the spatial distribution of photosynthetic capacity in a canopy) to be inferred from a more easily measured and/or simulated physical property (the distribution of light). Under certain limiting conditions, it even makes leaf-scale models of photosynthesis scale-invariant, meaning that the models work whether applied using leaf-level parameters or their canopy-level averages (Farquhar, 1989).

Those predictions from optimality theory contrast starkly with observations. Abundant data across many species and functional types show that the ratio of photosynthetic capacity between shaded and sunlit layers systematically exceeds the ratio of irradiance; that is, more sunlit canopy locations have less photosynthetic capacity per unit irradiance (e.g. Hirose & Werger, 1987; Evans, 1993; Hollinger, 1996; de Pury & Farquhar, 1997;

Table 1 Mathematical symbols, units and default values; annotations in default value denote C pools (L, leaves; R, roots; S, stem); asterisks denote parameters adjusted in the sensitivity analysis.

Description	Symbol	Units	Default value
Net CO_2 assimilation rate	A	μmol m^{-2} s^{-1}	–
Leaf absorptance to photosynthetically active radiation	α	–	–
Canopy net carbon gain	A_c	mol s^{-1}	–
Leaf area per unit carbon	a_{cL}	m^2 mol^{-1}	0.2398*
Ground area accessed by root system	a_g	m^2	3.14 (π)
A limited by RuBP carboxylation (j = V) or regeneration (j = J)	A_j	μmol m^{-2} s^{-1}	–
Total assimilation rate of module m	$A_{T(m)}$	μmol s^{-1}	–
Time-averaged net CO_2 assimilation rate	$\langle A \rangle$	μmol m^{-2} s^{-1}	–
Effective overhead cost per unit carbon for pool j	β_j	mol mol^{-1} s^{-1}	–
Ambient CO_2 mole fraction	c_a	μmol mol^{-1}	415*
Sensitivity of Chl to N_C	χ_c	μmol m^{-2} s^{-1} mmol^{-1}	0.03384
Sensitivity of Chl to N_J	χ_{cj}	μmol m^{-2} s^{-1} mmol^{-1}	4.64×10^{-4}
Leaf Chl content	Chl	mmol m^{-2}	–
Intercellular CO_2 mole fraction	c_i	μmol mol^{-1}	–
Carbon in functional pool j	C_j	C	–
Sensitivity of J_M to N_J	χ_J	μmol m^{-2} s^{-1} mmol^{-1}	9.48
Heat capacity of air	c_{pa}	J mol^{-1} K^{-1}	–
Total carbon in roots and stem modules	C_{TOTAL}	mol	40*
Sensitivity of V_M to N_V	χ_V	μmol m^{-2} s^{-1} mmol^{-1}	4.49
Leaf to air water vapor mole fraction gradient	Δw	mol mol^{-1}	–
Transpiration rate	E	mol m^{-2} s^{-1}	–
Atmospheric emissivity	ϵ_a	–	–
Leaf emissivity	ϵ_L	–	0.97
Total transpiration rate of canopy module m	$E_{T(m)}$	mol s^{-1}	–
Effective quantum yield of electrons	Φ	–	–
Fraction of net carbon gain used in construction respiration	f_c	–	0.28*
IR exchange as fraction of value above canopy	f_{IR}	–	–
Ratio of nocturnal to diurnal leaf respiration rate	f_{rdn}	–	0.864*
Maximum quantum yield of photosystem II	$\phi_{PSIImax}$	–	–
Boundary layer conductance to water CO_2	g_{bc}	mol m^{-2} s^{-1}	–
Boundary layer conductance to heat	g_{bh}	mol m^{-2} s^{-1}	2
Boundary layer conductance to water vapor	g_{bw}	mol m^{-2} s^{-1}	–
Fraction of N withdrawn from pool j before senescence	γ_j	–	0.5 (L,S), 0 (R)*
Stomatal conductance to CO_2	g_{sc}	mol m^{-2} s^{-1}	–
Stomatal conductance to water vapor	g_{sw}	mol m^{-2} s^{-1}	–
Photorespiratory CO_2 compensation point	Γ_*	μmol mol^{-1}	–
Incident irradiance	I	μmol m^{-2} s^{-1}	–
Potential electron transport rate	J	μmol m^{-2} s^{-1}	–
Maximum potential electron transport rate	J_M	μmol m^{-2} s^{-1}	–
Total hydraulic conductance from soil to a module	K	mol s^{-1} MPa^{-1}	–
Canopy extinction coefficient for visible light	k_i	–	0.56*
Hydraulic conductance of functional pool j	K_j	mol s^{-1} MPa^{-1}	–
Leaf hydraulic conductance	K_{leaf}	mol m^{-2} s^{-1} MPa^{-1}	0.01146*
Hydraulic conductance per unit fine root carbon	κ_R	mol s^{-1} MPa^{-1} mol^{-1}	6.6×10^{-4}*
C_R (per ground area) at which U_N is half its maximum	k_{nR}	mol m^{-2}	16*
Factor influencing hydraulic conductance per unit stem C	k'_S	mol m^2 s^{-1} MPa^{-1} mol^{-1}	0.00979*
Effective Michaelis constant for RuBP carboxylation	K'	μmol mol^{-1}	–
Axial stem length of a module	L	m	1
Leaf area of module	L	m^2	1
Latent heat of vaporization	Λ	J mol^{-1}	4.4×10^4
Target value of marginal carbon revenue of nitrogen	μ_n	μmol mmol^{-1}	–
Target value of marginal carbon revenue of water	μ_w	μmol mmol^{-1}	–
Leaf photosynthetic N content	N	mmol m^{-2}	–
Leaf N invested in light capture	N_C	mmol m^{-2}	–
N : C ratio of fine roots (j = R) or sapwood (j = S)	n_{cj}	mmol mol^{-1}	17 (R), 1.2 (S)*
Leaf N invested in electron transport and RuBP regeneration	N_J	mmol m^{-2}	–
Rate of N inputs into the soil per unit ground area	N_M	mmol yr^{-1}	400*
Leaf N invested in RuBP carboxylation	N_V	mmol m^{-2}	–
Rate of N loss due to senescence of pool j	N_{sj}	mmol s^{-1}	–
Total N in module m	$N_{T(m)}$	mmol	–

Table 1 (Continued)

Description	Symbol	Units	Default value
Total canopy N content	N_{TOTAL}	mmol	–
Vector of functional N pools	**P**	–	–
Whole plant carbon profit	P	mol s^{-1}	–
Atmospheric pressure	P_A	Pa	101325
Shortwave radiation	Q	J m^{-2} s^{-1}	–
Convexity parameter for colimitation of A by A_V and A_J	θ_A	–	0.999
Convexity parameter for response of J to irradiance	θ_J	–	–
Risk of death at a given water potential	R	–	–
Rate of non–photorespiratory CO_2 release (d = day, n = night)	R_d, R_n	μmol m^{-2} s^{-1}	–
Ambient relative humidity	RH	–	0.5
Maintenance respiration per unit carbon of pool j	r_j	mol mol^{-1} yr^{-1}	0.72 (R), 0.0072 (S)*
Hydraulic resistance of pool j	R_j	MPa s mol^{-1}	–
Sapwood carbon density	ρ_{cS}	mol m^{-3}	22995*
Ratio of nightlength to daylength	ρ_{dn}	–	1*
Stefan–Boltzmann constant	σ_B	J m^{-2} s^{-1} K^{-4}	5.67×10^{-8}
Senescence rate per unit carbon for pool j	s_j	mol mol^{-1} yr^{-1}	$1/\tau_j$
Air temperature	T_A	deg C	25
Air temperature in kelvins	T_{AK}	K	298.15
Lifespan of functional pool j	τ_j	y	1 (L,R), 11.6 (S)*
Leaf temperature	T_L	deg C	–
Effective no. of seconds per year of active photosynthesis	t_P	s yr^{-1}	5×10^{6}*
Rate of N uptake by fine roots	U_N	mmol s^{-1}	–
Maximum RuBP carboxylation velocity	V_m	μmol m^{-2} s^{-1}	–
V_m corrected to 25°C	V_{m25}	μmol m^{-2} s^{-1}	–
Ambient water vapor mole fraction	w_A	mol mol^{-1}	0.0316
Saturated water vapor mole fraction	w_s	mol mol^{-1}	–
Vector of canopy positions	**X**	–	–
Slope parameter for risk function	ξ	MPa^{-1}	5
Value of ψ_L causing runaway loss of hydraulic conductivity	ψ_c	MPa	–
Leaf water potential	ψ_L	MPa	–
Soil water potential	ψ_{soil}	MPa	0
Value of water potential at which risk is 0.5	ψ_{50}	MPa	–2.0*
Stem taper term	ζ_S	–	0.38*

Makino *et al.*, 1997; Bond *et al.*, 1999; Friend, 2001; Frak *et al.*, 2002; Kull, 2002; Lloyd *et al.*, 2010; Niinemets *et al.*, 2015; Hikosaka *et al.*, 2016; Salter *et al.*, 2020). No single hypothesis seems adequate to explain this apparent divergence between theory and observations across all environments and functional types (Niinemets, 2012; Buckley *et al.*, 2013; Niinemets *et al.*, 2015; Hikosaka *et al.*, 2016) – posing a puzzle for physiologists and ecologists, and casting doubt on the theory and its utility for predicting and interpreting plant function.

Most theoretical studies of canopy N partitioning have used models in which spatial variation in photosynthesis is driven solely by patterns of N and light, and have thus overlooked the potential influence of spatial patterns of water loss on photosynthetic N economy (Buckley *et al.*, 2002). It has long been known that stomatal conductance is often systematically suppressed in upper-canopy leaves (Ryan & Yoder, 1997; Delzon *et al.*, 2004; Koch *et al.*, 2004). Such suppression would cause optimal photosynthetic capacity to be lower than expected in the upper canopy (Peltoniemi *et al.*, 2012; Buckley *et al.*, 2013), and could arise from low leaf water potentials, caused either by the greater hydraulic resistance encountered in transporting water to more distal sites in the canopy, or by elevated evaporative demand in more sunlit locations (Ambrose *et al.*, 2016; Bachofen *et al.*, 2020). Indeed, stomatal conductance responds negatively both to reduced water potential and increased evaporative demand (Buckley, 2019).

Yet the empirical fact of reduced stomatal conductance in the upper canopy does not by itself resolve the apparent failure of optimization theory. Why would a plant not simply provide sunlit leaves with greater capacity for water transport, to prevent reductions in water potential – and hence stomatal conductance and optimal photosynthetic capacity – resulting from height, transport distance, or evaporative demand? Peltoniemi *et al.* (2012) found that stomatal conductance and photosynthetic capacity should not in fact be suppressed in the upper canopy if hydraulic conductance were optimally distributed between canopy modules, which suggests that hydraulic conductance is not optimally distributed in real plants. Similarly, Buckley *et al.* (2014) found that the spatial distribution of stomatal conductance and water loss was systematically suboptimal in grapevine canopies, with sunlit leaves transpiring less than predicted and shaded leaves transpiring more.

The latter result was premised on the same logic as Eqn 1: namely, if one assumes that a given total amount of water loss is available for distribution in the canopy, then, provided water use earns carbon gain with diminishing returns ($\partial^2 A/\partial E^2 < 0$),

canopy carbon gain is maximized if the marginal carbon revenue of water $((\partial A/\partial g_{sw})/(\partial E/\partial g_{sw}) \equiv \partial A/\partial E)$ is invariant and equal to a Lagrange multiplier, μ_w:

$$\frac{\partial A}{\partial E}(\mathbf{x}, t) = \mu_w \qquad \text{Eqn 2}$$

where E is transpiration rate, g_{sw} is stomatal conductance to H_2O, and t is time (Buckley *et al.*, 2002). (Cowan & Farquhar (1977) derived a result identical to Eqn 2; although they focused on invariance of $\partial A/\partial E$ over time, rather than among leaves in a canopy, the domain of variation does not affect the mathematical validity of the solution; Buckley *et al.*, 2002.) The conclusion of Peltoniemi *et al.* (2012) was likewise premised on the assumption that the total hydraulic conductance (K) is an imposed constraint, such that $\partial A/\partial K$ should be invariant in the optimum.

My objective here was to determine whether the assumptions that $\partial A/\partial E$ and $\partial A/\partial K$ should be spatially invariant in the optimum are consistent with a broader interpretation of optimization theory, in which the problem is extended to a higher level of organization: namely, optimal carbon partitioning at the whole-plant level, subject to biophysical and economic constraints on leaf water potential. I used simulations from a whole-plant model to test the hypothesis that spatial invariance in $\partial A/\partial N$, $\partial A/\partial E$ and $\partial A/\partial K$, and by extension, invariance in optimal photosynthetic capacity per unit incident irradiance between sunlit and shaded regions of the canopy, does in fact emerge from optimal carbon partitioning.

Description

Overview

I simulated canopy photosynthesis in an imaginary plant consisting of a root system and two canopy modules (one 'sunlit' and one 'shaded', the latter having lower leaf-level incident irradiance than the former; note that this differs from the use of 'sunlit' and 'shaded' to describe regions of a given leaf layer that are in sunflecks and shadeflecks, respectively). Each canopy module includes a stem carbon pool and a fixed amount of leaf area. I assigned each module three other parameters: incident irradiance (i), boundary layer conductance to heat (g_{bh}) and axial stem length (l); I assumed air temperature and relative humidity were identical between modules. In this model, stem carbon determines each module's total xylem conducting area and thus stem hydraulic conductance (see Eqn 7 below), and root carbon determines the root hydraulic conductance shared by both modules (Eqn 6), as well as the total supply of nitrogen available (Eqn 16). I maximized carbon profit (P, defined as canopy photosynthesis (A_c, the sum of photosynthesis in both modules) minus the amortized carbon costs of maintenance and turnover of the carbon pools) by numerically adjusting the following: the partitioning of a fixed total carbon supply, C_{TOTAL}, among the root and stem carbon pools; the partitioning of available N between the two canopy modules, and among N pools for ribulose 1,5-bisphosphate (RuBP) carboxylation, electron transport and light capture in each module; and the values of leaf water potential in each module. (Note that this model diverges from common modeling practice in adjusting water potential and calculating stomatal conductance from the resulting transpiration rate, rather than the converse.) I recorded how gas exchange parameters that emerged from the optimization in each module compared to one another in relation to the ratio of irradiance between the two modules. I repeated this procedure for a range of conditions and assumptions (see the 'Simulations' subsection, below, and Table 2).

Degrees of freedom

The model has nine biological degrees of freedom (dfs), excluding parameters treated as constants. There are 15 variables: root carbon, plus seven variables for each of two modules (three N pools, irradiance, stomatal conductance, water potential and stem carbon). Two dfs are removed by specifying incident irradiance for each module; one df is removed by constraining the sum of the remaining C pools to a constant; stomatal conductance is constrained by carbon pools and water potentials (Eqn 11 below), removing two dfs; and total N available to the canopy is constrained by carbon pools (Eqn 16 below), removing one df. Of the nine remaining dfs, seven can be expressed as partitioning fractions (two for C and five for N), and two represent the leaf water potential in each module. Fig. 1(a) illustrates the logical and causal relationships among major terms in the model.

Timescale

Because this analysis was intended to focus on long-term adjustment of N and C partitioning in the canopy in relation to biophysical limits on leaf water potential, the timescale of these simulations is implicitly on the same order as that of N and C partitioning (i.e. weeks or months). Thus, diurnal variation in stomatal conductance, water potential, irradiance and other environmental factors is not considered. The conditions in which gas exchange is calculated in the model are best interpreted as midday conditions, in which leaf water potential is most negative and thus most unambiguously constrained by the risk of catastrophic xylem failure (as discussed later in the subsection 'Penalizing the non-stomatal consequences of low leaf water potential').

The model

Canopy net carbon gain (Ac) is the sum of total carbon gain ($A_{T(m)}$) in each canopy module m (m = 1 or 2 in this study), which in turn is the product of leaf area ($L_{(m)}$) and photosynthesis per unit leaf area ($A_{(m)}$) for that module, minus the effective nocturnal leaf respiration rate, $R_{n(m)}$:

$$A_c = \sum_m A_{T(m)} = \sum_m L_{(m)}\left(A_{(m)} - \rho_{dn} R_{n(m)}\right) \qquad \text{Eqn 3}$$

where ρ_{dn} is the ratio of nightlength to daylength, which adjusts $R_{n(m)}$ (assumed to be a fixed fraction, f_{rnd}, of daytime leaf

Table 2 List of simulations, with values or ranges of parameters adjusted in each.

Simulation	Boundary layer conductance (g_{bh})	Air temperature (T_A)	Relative humidity (RH)	Hydraulic pathlength of sunlit module (l_{sunlit})	Steepness parameter for risk curve (ξ)	Irradiance ratio (i_{shaded}/i_{sunlit})
Default	2 mol m^{-2} s^{-1}	25°C	50%	1 m	5 MPa^{-1}	0.13–1.0
Low g_{bh}	1	–	–	–	–	(i_{sunlit} = 1500 µ mol m^{-2} s^{-1};
High g_{bh}	1000	–	–	–	–	i_{shaded} = 200 – 1500)
Low g_{bh} in shaded	1*	–	–	–	–	
High T_A	–	35	–	–	–	
Low RH	–	–	25	–	–	
Long	pathlength	–	–	–	1.5, 2.0	
–						
Gradual risk	–	–	–	–	1	
Steep risk	–	–	–	–	∞	
Max A_c not P	–	–	–	–	–	

'–', parameter was set to default value given in first row; *g_{bh} was 1 and 2 mol m^{-2} s^{-1} in shaded and sunlit modules, respectively. The last row refers to a simulation using canopy carbon gain (A_c) rather than profit (P) as the goal function.

respiration $R_{d(m)}$) to the same time basis as $A_{(m)}$. Whole-plant carbon profit (P) is:

$$P = (1 - f_c)(A_c - t_P^{-1}\Sigma_j r_j C_j) - t_P^{-1}\Sigma_j s_j C_j \qquad \text{Eqn 4}$$

where f_c is the fraction of net allocatable carbon (i.e. net photosynthesis minus whole-plant maintenance respiration) lost to construction respiration when constructing the carbon pools, t_P is the effective number of seconds per year of active photosynthesis (which scales instantaneous photosynthesis rates to annual values), and r_j and s_j are the rates of maintenance respiration and senescence, respectively, per unit carbon for carbon pool j. I calculated s_j as the inverse of tissue lifespan, τ_j. (Note that r_j for leaf carbon pools is zero, because leaf maintenance respiration is already accounted for in calculation of A and R_n.)

Canopy photosynthesis is determined by three resources, or inputs: water (which limits stomatal conductance), nitrogen (which limits photosynthetic capacity and leaf absorptance), and light (the irradiance incident on each canopy module is treated as an input parameter in this model). The amount of water and N available to each module depends on the availability of those resources in the environment, but also on the sizes of functional carbon pools (roots, stems and leaves) that acquire and transport those resources. The next section describes models for those dependencies; the biochemical model of photosynthesis itself is presented in Appendix A1.

How carbon partitioning and water potential determine stomatal conductance

At steady-state and on average, mass conservation requires that the total transpiration rate of a module ($E_{T(m)}$) equals the rate of water transport from the soil to the module. The latter rate is determined by hydraulic conductances, which depend on C partitioning, and by soil and leaf water potentials. Because both modules share the root component of whole-plant hydraulic conductance (K_R), E_T in each module depends in part on the leaf water potential and total hydraulic conductance of the other module. The resulting expressions for E_{T1} and E_{T2}, derived in Supporting Information Methods S1, are:

$$E_{T1} = \frac{K_1(K_R(\psi_{soil} - \psi_{L1}) + K_2(\psi_{L2} - \psi_{L1}))}{K_R + K_1 + K_2}, \qquad \text{Eqn 5a}$$

$$E_{T2} = \frac{K_2(K_R(\psi_{soil} - \psi_{L2}) + K_1(\psi_{L1} - \psi_{L2}))}{K_R + K_1 + K_2}, \qquad \text{Eqn 5b}$$

in which $K_1 = (K_{S1}^{-1} + K_{L1}^{-1})^{-1}$ and $K_2 = (K_{S2}^{-1} + K_{L2}^{-1})^{-1}$, where $K_{S(m)}$ and $K_{L(m)}$ are the stem and leaf hydraulic conductances of module m, respectively. The hydraulic conductances depend on carbon in each pool:

$$K_R = \kappa_R C_R \qquad \text{Eqn 6}$$

$$K_{S(m)} = \frac{k'_S}{l^2_{(m)}} C_{S(m)} = \kappa_S C_{S(m)} \qquad \text{Eqn 7}$$

$$K_{L(m)} = L_{(m)} K_{leaf} \qquad \text{Eqn 8}$$

Equations 6 and 7 are derived in Methods S2; κ_R, k'_S and K_{leaf} are parameters that I treated as constants in this study, and $l_{(m)}$ is the hydraulic pathlength of canopy stem module m. (K_{leaf} is on a leaf-area basis; thus, Eqn 8 assumes that changes in leaf area, $L_{(m)}$, occur by addition or subtraction of leaves of fixed size, which are hydraulically in parallel with one another, thus increasing $K_{L(m)}$. However, since $L_{(m)}$ = 1 m^2 by definition for both modules in this study, $K_{L(m)}$ is constant and identical between modules.) The module transpiration rate must also equal the

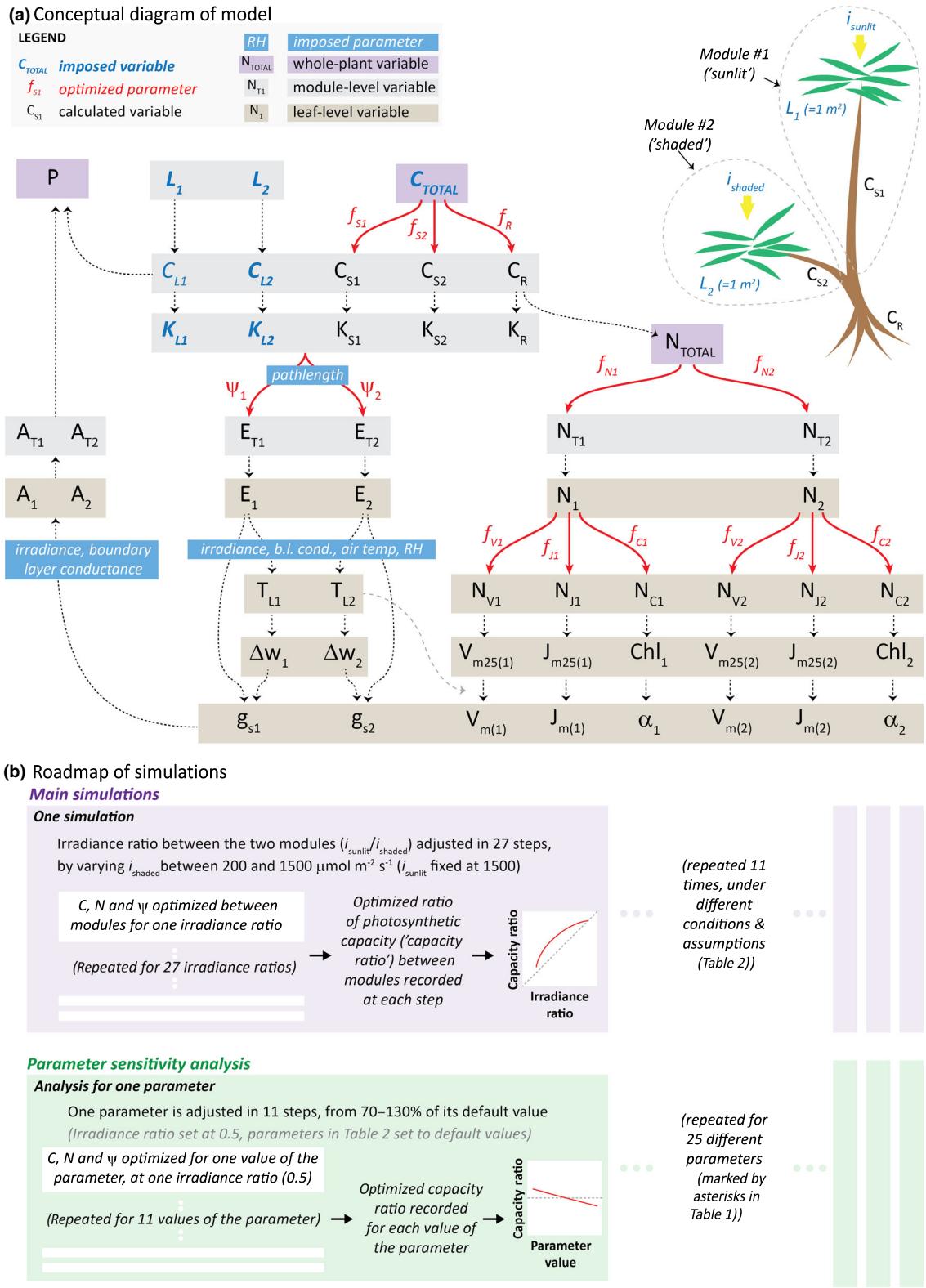

Fig. 1 (a) Conceptual diagram of the model. (b) Roadmap of simulations. *P*, *L*, *C*, *N* and *A* denote, respectively, profit, leaf area, carbon, nitrogen and assimilation rate; subscripts 1 and 2 denote modules, as shown at top right; other symbols are defined in Table 1.

product of module leaf area, total conductance to water vapor, and leaf to air water vapor mole fraction difference ($\Delta w_{(m)}$):

$$E_{T(m)} = L_{(m)} E_{(m)} = L_{(m)} \cdot \frac{g_{sw(m)} g_{bw(m)}}{g_{sw(m)} + g_{bw(m)}} \Delta w_{(m)} \quad \text{Eqn 9}$$

where g_{sw} and g_{bw} are stomatal and boundary layer conductances to H_2O, respectively. Δw depends on leaf temperature, T_L:

$$\Delta w_{(m)} = w_s(T_L) - w_A \quad \text{Eqn 10}$$

where w_A is the ambient water vapor mole fraction and $w_s(T)$ is the saturated water vapor mole fraction at a temperature T ($w_s(T) = 611.0032 \cdot \exp(17.62 \cdot T/(243.12 + T))/P_A$, where P_A is atmospheric pressure in Pa and w_s is in mol mol^{-1} (World Meteorological Organization, 2008)). $w_A = \text{RH} \cdot w_s(T_A)$, where RH is relative humidity as a fraction. I estimated T_L based on energy balance (Methods S3), which depends on absorbed radiation, air temperature, boundary layer conductance and transpiration rate E (from Eqn 9). The stomatal conductance in each module ($g_{sw(m)}$) is found by inverting Eqn 9:

$$g_{sw(m)} = \left(\frac{L_{(m)} \Delta w_{(m)}}{E_{T(m)}} - \frac{1}{g_{bw(m)}} \right)^{-1} \quad \text{Eqn 11}$$

where $E_{T(m)}$ is calculated from Eqn 5. $g_{sw(m)}$ is applied to Eqn A8 in Appendix A1 to calculate CO_2 assimilation rate.

Thus, in this model, stomatal conductance is determined by carbon partitioning (via the hydraulic conductances, which affect E_T), leaf water potential, and environmental parameters that affect Δw. Stem and root carbon partitioning fractions and water potentials are optimized numerically.

How carbon partitioning determines canopy N supply

I modeled the total supply of photosynthetic N available for partitioning between canopy modules (N_{TOTAL}) by assuming a steady-state between N uptake by roots (U_N) and losses due to tissue senescence. I modeled U_N following Buckley & Roberts (2006a), as:

$$U_N = a_g N_M \left(\frac{C_R/a_g}{C_R/a_g + k_{nR}} \right) = 2L_{(m)} N_M \left(\frac{C_R}{C_R + 2L_{(m)} k_{nR}} \right) \quad \text{Eqn 12}$$

where a_g is ground area, N_M is the rate of N inputs into the soil per unit ground area (mmol N m$^{-2}_{\text{ground}}$ s^{-1}), C_R is root carbon, and k_{nR} is the value of root C (per unit ground area) at which the rate of N uptake is half of N_M. I set a_g to twice the projected ground area of each canopy module, because the root system as modeled here supplies both modules. I modeled the N loss rate to leaf senescence as:

$$N_{sL} = \frac{1-\gamma_L}{\tau_L} N_{TOTAL} \quad \text{Eqn 13}$$

where τ_L is leaf lifespan (s) and γ_L is the fraction of N withdrawn from leaves before senescence. The N loss rates due to senescence of N-containing nonphotosynthetic tissues (roots and stems) are:

$$N_{sS(m)} = \frac{1-\gamma_S}{\tau_S} n_{cS} C_{S(m)} \quad \text{Eqn 14}$$

$$N_{sR} = \frac{1-\gamma_R}{\tau_R} n_{cR} C_R \quad \text{Eqn 15}$$

for stems and roots, respectively, where γ_j, τ_j and n_{cj} are the fractions of N withdrawn from pool j before senescence, the lifespan of the pool, and the N : C ratio of the pool, respectively. Setting $U_N - N_{sL} - N_{sS} - N_{sR}$ equal to zero and solving for N_{TOTAL} gives:

$$N_{TOTAL} = \frac{\tau_L}{1-\gamma_L} \left(\frac{2L_{(m)} N_M C_R}{C_R + 2L_{(m)} k_{nR}} \right) - \frac{1-\gamma_S}{1-\gamma_L} \left(\frac{\tau_L}{\tau_S} \right) n_{cS} (C_{S1} + C_{S2}) - \frac{1-\gamma_R}{1-\gamma_L} \left(\frac{\tau_L}{\tau_R} \right) n_{cR} C_R \quad \text{Eqn 16}$$

where C_{S1} and C_{S2} are stem carbon in canopy modules #1 and #2, respectively.

Thus, N_{TOTAL} is determined chiefly by root C, but also to a small degree by stem C. The partitioning of N_{TOTAL} between canopy modules, and among functional pools within each module, is optimized numerically in this model. The resulting functional N pools affect photosynthesis via carboxylation and electron transport capacities and leaf absorptance (Eqns A5–A7 in Appendix A1).

Penalizing the nonstomatal consequences of low leaf water potential

In the carbon balance model summarized above, maintaining a high leaf water potential is never beneficial for carbon gain, because any decrease in ψ_L leads directly to an increase in stomatal conductance (Eqn 11), and therefore an increase in carbon gain (Eqn A8). The main reason ψ_L does not generally become arbitrarily low in real plants is that doing so has negative consequences that are independent of stomatal conductance. (Plants have thus evolved to close stomata at low ψ_L; however, such adaptive responses cannot be taken as prior constraints if the objective, as in this study, is to identify adaptive responses.) Very low ψ_L leads to irreversible loss of water transport capacity (Tyree & Sperry, 1988, 1989; Choat *et al.*, 2012; McCulloh *et al.*, 2019) with consequent runaway desiccation. Although some nonstomatal consequences of low ψ_L, such as depression of photosynthetic capacity, can manifest directly in reduced photosynthesis (Lawlor & Tezara, 2009), most evidence suggests such effects are generally not substantial until water potential is already low enough to cause both stomatal closure and cavitation (Kaiser, 1987; Downton *et al.*, 1988; Sharkey & Seemann, 1989; Quick

et al., 1992; Centritto *et al.*, 2003; Koch *et al.*, 2004; Chaves *et al.*, 2009). As a result, most nonstomatal effects of low ψ_L on carbon balance are intrinsically probabilistic – they are driven by the risk of exceeding the threshold for runaway cavitation (ψ_c), rather than by immediate short-term carbon costs – so they influence the *expected value* of total carbon gain over the module's lifespan, $\langle A$, rather than the instantaneous assimilation rate, A. For these reasons, I modeled nonstomatal costs of low ψ_L using a nondimensional *risk factor* that is a function of ψ_L and is multiplied by the photosynthesis rate calculated in the absence of nonstomatal effects of ψ_L:

$$<A> = (1 - r(\psi_L)) \cdot A\big(g_{sw}(\psi_L)\big) \qquad \text{Eqn 17}$$

I assumed the risks represented by r varied sigmoidally with ψ_L, increasing from zero in an accelerating manner as ψ_L declines from zero towards a threshold value, ψ_{50}, at which $r = 0.5$, and then then decelerating as ψ_L declines further. A convenient function with these properties is:

$$r(\psi_L) = \frac{1 - \exp(-\xi\psi_L)}{2 - \exp(-\xi\psi_{50}) - \exp(-\xi\psi_L)} \qquad \text{Eqn 18}$$

where ξ controls the slope of the function at $\psi_L = \psi_{50}$ (large ξ = steep slope). Note that ψ_L and $\psi_{50} \leq 0$ for Eqn 18.

The formulation represented by Eqns 17–18 is very similar to those adopted in recent optimization based models of stomatal conductance, in which r represents the hydraulic vulnerability curve (e.g. Wolf *et al.*, 2016; Sperry *et al.*, 2017; Eller *et al.*, 2020). In this model, however, r is not the hydraulic vulnerability curve, but rather the risk of catastrophic desiccation posed by allowing ψ_L to reach a given value. That risk is influenced by the vulnerability curve, but also by factors that affect the likelihood of transiently exceeding ψ_c, such as how quickly stomata can respond to fluctuations in evaporative demand, and the probability distribution of such fluctuations. It is beyond the scope of this study to characterize rigorously the relationship between the vulnerability curve and the risk function – that would require detailed modeling of non-steady-state gas exchange over a long period, driven by high-frequency environmental data. Since the risk function is thus uncertain, I included several simulations to assess how its properties influence predicted canopy scaling of photosynthetic capacity in relation to light. The parameter ψ_{50} is also among those included in a parameter sensitivity analysis described under 'Parameter values and sensitivity analysis'.

Simulations

A 'roadmap' of the simulations performed in this study is shown in Fig. 1(b). I adjusted the model's nine degrees of freedom numerically using the 'optim()' function in base R to maximize either whole-plant carbon profit or total photosynthesis (in each case using the expected values of assimilation rate given by Eqn 17). I repeated this procedure for a range of parameter combinations (Table 2). In each simulation, I calculated $\partial A/\partial E$, $\partial A/\partial N$, $\partial A/\partial K$ and $\partial P/\partial N$ numerically for each module. Details of the optimization procedure, R code, and an input parameter file are provided as Methods S4–S6, respectively. Verification that the identified optima were global is presented in Figs S1 and S2.

The simulations included three scenarios for the steepness of the risk curve (controlled by the parameter ξ in Eqn 18): two finite values of ξ (1 and 5 MPa^{-1}) and one scenario representing the limit of large ξ. In the large- ξ scenario, I simply set ψ_L to ψ_{50} and excluded ψ_L from the list of parameters to optimize; this was because, under large ξ, r is equal to 1 for all $\psi_L \geq \psi_{50}$ and equal to zero for $\psi_L < \psi_{50}$, so that $\langle A$ is by definition greatest in the limit of $\psi_L \rightarrow \psi_{50}$ – making numerical optimization of ψ_L unnecessary.

Parameter values and sensitivity analysis

Biological and environmental parameters and their default values are listed in Tables 1 and 2. I estimated biological parameters from a variety of literature sources, as described in Methods S7. I chose values for total carbon supply, soil N input rate, and ground area per module to produce reasonable values for key gas exchange parameters. In the simulations described below, I used the 'nominal' values given for each parameter unless otherwise stated. Given the large variability and/or uncertainty in some of the model's parameters, I performed a parameter sensitivity analysis by varying certain parameters (those marked with an asterisk in Table 1) between 70% and 130% of their default values and recording how the resulting optimal ratio of photosynthetic capacity between the shaded and sunlit canopy modules varied.

Results

When carbon partitioning was optimized in a plant model with two canopy modules (one 'sunlit' module with greater irradiance, i, than the other 'shaded' module), the ratio of photosynthetic capacity between the shaded and sunlit modules exceeded the ratio of irradiance (Fig. 2; Table 3 gives values for a number of gas exchange-related parameters for a single simulation in which irradiance in the sunlit module was twice that in the shaded module). In other words, a plot of the capacity ratio on the vertical axis and the irradiance ratio on the horizontal axis systematically diverged above the 1 : 1 line (thick grey line in Fig. 2). This divergence was generally greatest at intermediate and high irradiance ratios. These results held, regardless of how photosynthetic capacity was quantified (as V_m or J_m; Fig. 2), though the divergence was slightly smaller for V_m than for J_m. Subsequent results are presented in terms of V_m (corrected to a common temperature of 25°C).

Evaporative demand (Δw) was typically greater in the sunlit module than in the shaded module (Fig. 3a,b), due to the greater radiation load in the sunlit module, except at low ambient relative humidity (25% vs the default of 50%) and in some cases at very low irradiance ratios (< 0.3). These differences in Δw moderately increased the positive divergence of the capacity ratio from the irradiance ratio (Fig. 3c,d). For example, differences in Δw between the modules were greater when boundary layer conductance (g_{bh}) was greater in the sunlit module (Fig. 3a) or air

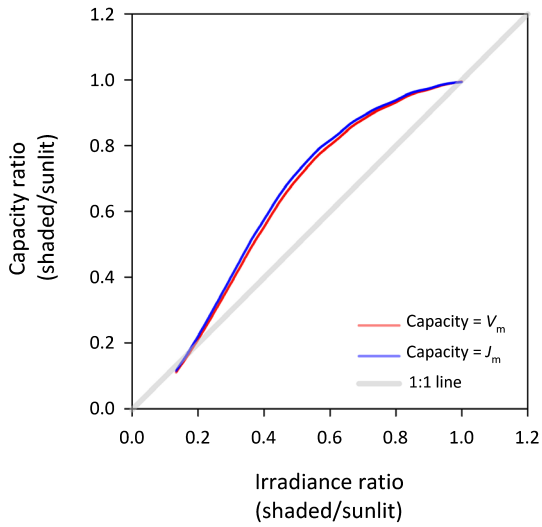

Fig. 2 The predicted optimal ratio of photosynthetic capacity (ribulose 1,5-bisphosphate (RuBP) carboxylation capacity (V_m, red line) or electron transport capacity (J_m, blue line)) between shaded and sunlit modules systematically exceeded the ratio of incident irradiance between the modules, when carbon partitioning was adjusted among roots and stem C pools in both modules so as to maximize whole-plant carbon profit. (The trend for CO_2- and light-saturated assimilation rate (A_m) was nearly identical to that for J_m, so the two could not be distinguished in a figure and hence only J_m is shown. Subsequent figures show results for V_m, temperature corrected to 25°C (V_{m25})).

Table 3 Detailed results for example simulation with irradiance ratio = 0.5 (i = 1500 and 750 μmol m^{-2} s^{-1} in sunlit and shaded modules, respectively) and default parameters; units for $\partial A/\partial E$, $\partial A/\partial N$, $\partial P/\partial N$ are μmol mmol^{-1}.

Variable	Sunlit	Shaded
V_m	112.3	78.6
J_m	178.4	128.4
A	23.9	17.1
c_i	270.7	277.9
g_{sw}	0.296	0.216
E	0.00409	0.00304
T_L	25.05	24.92
Δw	0.0157	0.0154
ψ_L	–1.45	–1.36
$\partial A/\partial E$	2.10	1.76
$\partial A/\partial N$	0.338	0.329
$\partial P/\partial N$	0.213	0.213

temperature was increased (Fig. 3b), and this translated into a greater divergence of the capacity and irradiance ratios (Fig. 3c, d). However, a substantial divergence persisted even if differences in Δw were eliminated by setting the boundary layer conductance to a very large value (ensuring that leaf and air temperatures were equal) (red lines in Fig. 3a,c).

In simulations in which the sunlit module was hydraulically distal to the shaded module – that is, water was required to travel farther to reach the sunlit module – optimal photosynthetic capacity was predicted to be greater in the shaded module, even if irradiance was as much as 50% greater in the sunlit module (Fig. 4).

The divergence of the capacity and irradiance ratios was inversely related to the steepness of the risk function used to penalize low leaf water potentials. For example, the divergence was slightly greater if risk was assumed to increase very gradually as ψ_L declined (Fig. 5; inset shows the risk function itself). However, the divergence persisted, except at low irradiance ratios, even if the risk function was infinitely abrupt (Fig. 5).

The patterns of photosynthetic capacity vs irradiance (shown in Figs 2–5) also gave rise to systematic differences in other parameters between the two modules. For example, intercellular CO_2 concentration (c_i) was greater in the shaded module than in the sunlit module, and the ratio of c_i between the two modules increased as the ratio of irradiance decreased (Fig. 6). Similarly, the predicted optimal values of the marginal carbon products of water ($\partial A/\partial E$) and hydraulic conductance ($\partial A/\partial K = (\partial A/\partial E)\cdot(\partial E/\partial K) \approx (\partial A/\partial E)\cdot(\psi_{soil} - \psi_L)$) were smaller in the shaded module than in the sunlit module; $\partial A/\partial K$ decreased more steeply in the canopy than $\partial A/\partial E$ because ψ_L was less negative in shaded modules than in sunlit modules (Fig. 6). The value of the marginal carbon product of nitrogen ($\partial A/\partial N$) differed slightly between the two modules, but the marginal effect of N on carbon profit ($\partial P/\partial N$) was always equal between the two modules (Fig. 6).

All results described above used whole plant carbon profit as the goal function for optimization of C and N partitioning and adjustment of leaf water potential. However, very similar patterns were predicted (with slightly reduced divergence of the capacity and irradiance ratios) if the goal function was instead taken as total canopy photosynthesis (the sum of contributions from the two modules) instead of carbon profit (Fig. S3). In those simulations, it also emerged that $\partial A/\partial N$ was invariant among modules in the optimum.

Predictions from the simulations described above were broadly consistent with published experimental data for irradiance ratios above approx. 0.4, but the predicted capacity ratio was generally lower than observed data for lower irradiance ratios (Fig. 7).

Parameter sensitivity analysis found that most parameters had little effect on the optimal capacity ratio (at an intermediate irradiance ratio of 0.5). Notable exceptions included key hydraulic parameters (ψ_{50}, K_{leaf} and κ_R), key parameters involving nitrogen balance (N_M, k_{Rn} and n_{cR}), and ambient [CO_2] (c_a); varying these parameters across a range equal to 60% of their default values led to changes of 21–28% in the optimal capacity ratio (Fig. S4). For five parameters (ψ_{50}, N_M, k_{Rn}, n_{cR} and τ_r), carbon profit went to zero within the examined range of the parameter (namely at low ψ_{50}, N_M and τ_r, and high k_{nR} and n_{CR}).

Discussion

Canopy profiles of photosynthetic capacity predicted by optimization theory have long been thought to contradict observations: leaves in shaded locations are thought to have too much photosynthetic capacity relative to their light availability, and conversely, sunlit leaves have too little capacity (recently reviewed by Niinemets *et al.*, 2015; Hikosaka *et al.*, 2016). I extended the theory to encompass not only optimal N partitioning among and within leaves, but

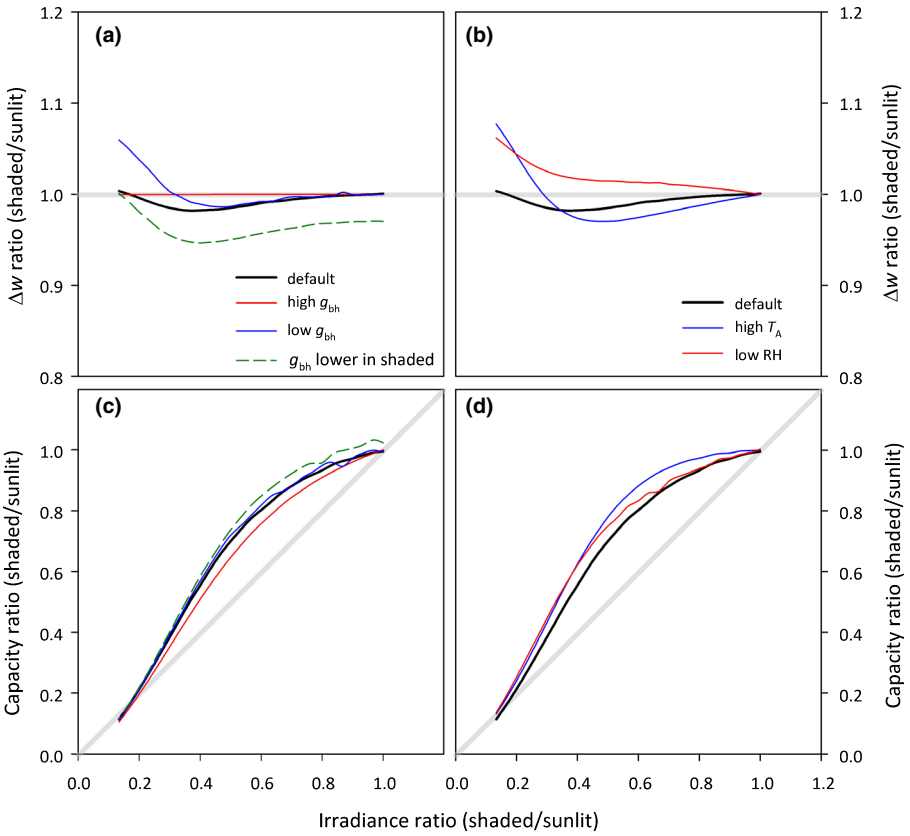

Fig. 3 (a, b) The evaporative demand (Δw; leaf to air water vapor mole fraction gradient) was generally lower in the shaded canopy module than in the sunlit module unless leaf temperature was effectively forced to equal air temperature by setting boundary layer conductance to heat to an extremely high value ('high g_{bh}', g_{bh} = 1000 mol m^{-2} s^{-1}). Either reducing g_{bh} from 2 (default) to 1 mol m^{-2} s^{-1} ('low g_{bh}'), setting g_{bh} lower in the sunlit module (g_{bh} = 1 mol m^{-2} s^{-1}, vs 2 mol m^{-2} s^{-1} in the sunlit module) or increasing air temperature from T_A = 25°C (default) to 35°C ('high T_A') magnified the difference in Δw between the two modules, whereas reducing relative humidity from RH = 50% (default) to 25% ('low RH') had the opposite effect. (c, d) In most cases, conditions that increased differences in Δw between modules also increased the divergence of the capacity and irradiance ratios. (Capacity ratio is expressed in terms of V_{m25}.) Diagonal grey lines in (c, d) are 1 : 1 lines.

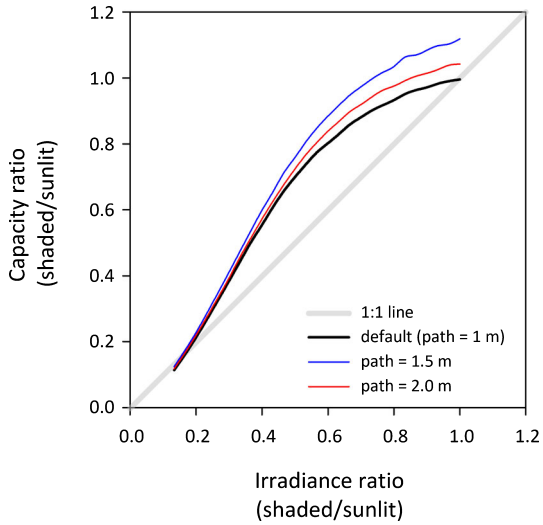

Fig. 4 Assigning the sunlit canopy module a greater hydraulic pathlength (l_1 = 1.5 or 2.0 m, blue and red lines, respectively) than the default value (l_1 = 1.0 m, black line) caused the capacity ratio to exceed the irradiance ratio by a greater degree, even if both modules had the same incident irradiance (irradiance ratio = 1.0).

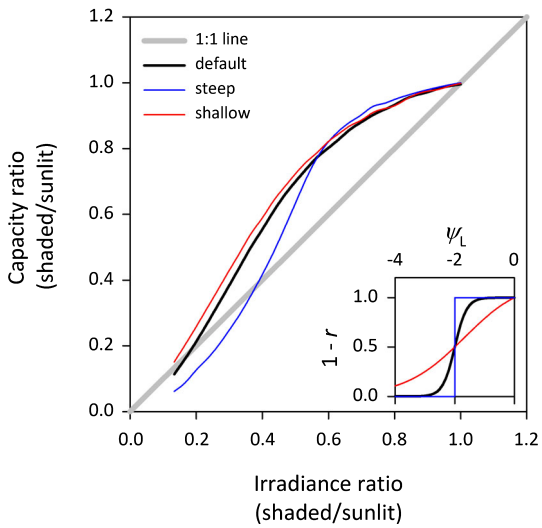

Fig. 5 The divergence of the ratio of photosynthetic capacity between canopy modules from the irradiance ratio was greater if the risk function (r) used to penalize low water potentials (Eqn 18, shown inset as $1 - r$ vs ψ_L) was less steep (red lines; $\xi = 1$ MPa^{-1}), and conversely, the divergence was smaller if the risk function was infinitely steep (blue lines; $\xi \to \infty$), relative to the default simulation (black lines; $\xi = 5$ MPa^{-1}).

also optimal carbon partitioning among functional C pools in the plant, while accounting for constraints on leaf water potential imposed by the risk of catastrophic desiccation. The patterns of within-canopy gas exchange that emerged from the resulting optimization are broadly similar to observations (Fig. 7). This result suggests that optimization theory does not in fact contradict observations regarding canopy profiles of gas exchange parameters.

Why does optimal carbon partitioning lead to variation in $\partial A/\partial E$ within the canopy?

I found that it is not optimal for $\partial A/\partial E$ to be invariant within a canopy, contrary to my own previous assertions (Buckley *et al.*,

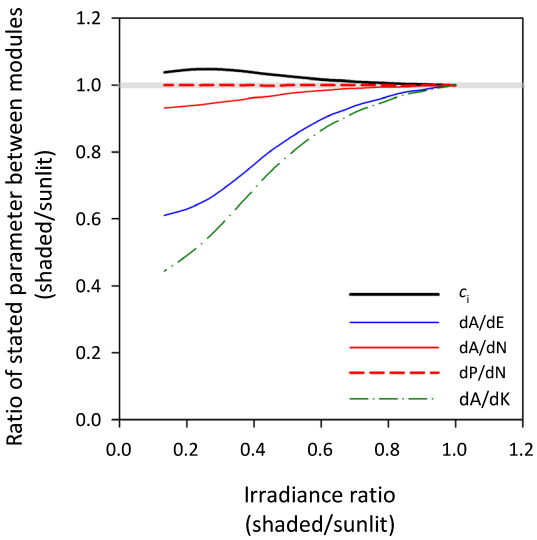

Fig. 6 Other parameters of gas exchange differed systematically between canopy modules when carbon (C) partitioning was adjusted among roots and stem C pools in both modules so as to maximize whole-plant C profit. Intercellular CO_2 concentration (c_i, black line) was greater in the shaded module; the marginal C revenues of water ($\partial A/\partial E$, blue line) and hydraulic conductance ($\partial A/\partial K$, green dash-dot line) were both smaller in the shaded module, and the marginal C revenue of nitrogen ($\partial A/\partial N$, solid red line) was slightly smaller in the shaded module. However, the marginal C profit of nitrogen ($\partial P/\partial N$, dashed red line), which accounts for the C cost of nocturnal leaf respiration, was invariant through the canopy.

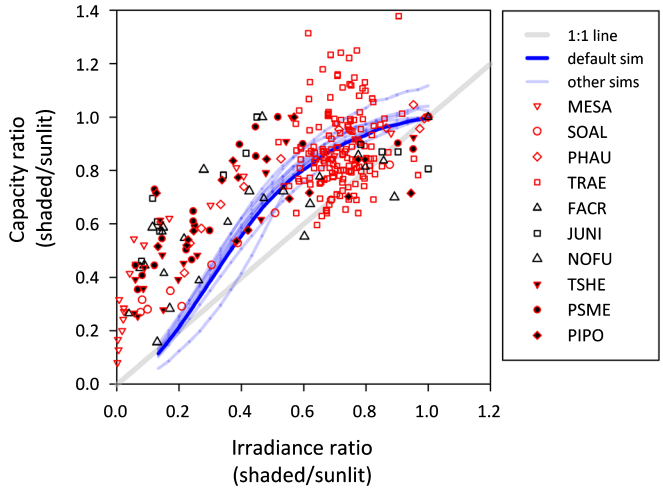

Fig. 7 For large and intermediate ratios of incident irradiance between shaded and sunlit canopy modules, the simulations presented in this study (blue lines) are broadly consistent with experimental measurements from a range of species and environments (symbols). The solid blue line shows the default simulation from the present study; the dashed blue lines are the other simulations, reprinted from Figs 2, 3(b), 4 and 5. Symbol coloring indicates species type (open red, herbaceous angiosperm; open black, woody angiosperm; closed red/black, woody gymnosperm). Species codes in the legend are as follows: MESA (*Medicago sativa*) (Louarn *et al*., 2015), SOAL (*Solidago altissima*) (Hirose & Werger, 1987; Hirose *et al*., 1988), PHAU (*Phragmites australia*) (Hirose & Werger, 1994, 1995), TRAE (*Triticum aestivum*) (Salter *et al*., 2020), FACR (*Fagus crenata*) (Iio *et al*., 2005), JUNI (*Juglans nigra* × *regia*) (Frak *et al*., 2002), NOFU (*Nothofagus fuscata*) (Hollinger, 1996), TSHE (*Tsuga heterophylla*) (Bond *et al*., 1999), PSMA (*Pseudotsuga menziesii*) (Bond *et al*., 1999), PIPO (*Pinus ponderosa*) (Bond *et al*., 1999). For MESA, capacity = electron transport capacity; for TRAE, capacity = light and CO_2-saturated assimilation rate; for all other species, capacity = light-saturated assimilation rate at ambient CO_2. Data for FACR, SOAL and PHAU were reproduced from Niinemets *et al*. (2015). All data were digitized from figures in the articles cited herein using WebPlotDigitizer (Rohatgi, 2020).

2002, 2014; Farquhar *et al*., 2002). To understand why, it helps to examine the Lagrange multiplier approach to optimization, which gave rise to my earlier assertions. In that approach, the optimum is found by setting the derivative of total photosynthesis with respect to stomatal conductance, g_{sw}, equal to zero. The total supply of water – the total transpiration rate – is considered constant. Because the supply is constant, its derivative with respect to g_{sw} is zero, so it can be multiplied by an arbitrary constant (the Lagrange multiplier) and subtracted from photosynthesis without affecting the location of the optimum.

An often-tacit assumption of this approach is that the resource can be redistributed arbitrarily. That is, any leaf can have any transpiration rate, as long as the total for all leaves adds up to some imposed constant. However, that assumption is not valid for canopy transpiration, because water use by canopy elements is constrained by factors that cannot themselves vary arbitrarily. These include leaf water potential (ψ_L), which is limited by fundamental biophysical constraints, and by root, stem and leaf hydraulic conductances, which depend on carbon investments. The transpiration rate E of a canopy module is approximately:

$$E \approx K(\psi_{soil} - \psi_L), \qquad \text{Eqn 19}$$

where ψ_{soil} is soil water potential and K is the total hydraulic conductance between the soil and the canopy module, including contributions from the module's own stem tissues. Neither K nor ψ_L can vary arbitrarily as needed to allow transpiration rate to take on any possible value in any given leaf. Leaf water potential is not free to vary arbitrarily, for two reasons. First, it is constrained to remain above a critical threshold, ψ_c, below which runaway loss of hydraulic conductivity becomes certain (Tyree & Sperry, 1989). Any strategy that leads to certain death is obviously inconsistent with the premise of optimization theory, so we must adopt the constraint that $\psi_L > \psi_c$. Second, economics also constrains how water potential can vary above ψ_c. Imagine a canopy module in which ψ_L were always well above ψ_c (even allowing for a 'safety margin', discussed in the next paragraph). If water potential were then allowed to decline somewhat while remaining safely above ψ_c, the rate of water transport to that module – and hence the transpiration rate, stomatal conductance and assimilation rate – would increase, without any cost to the plant. Therefore, having leaf water potential remain permanently above a safe lower limit is inherently suboptimal with respect to carbon gain.

Two counterarguments arise from game-theoretical considerations, but neither contradicts the arguments above. Firstly, it could be beneficial for a plant to keep ψ_L high to conserve water under some circumstances (for example, banking soil water stores for later in the season, or to mitigate the risk of fatal desiccation in droughts of uncertain duration) (Cowan, 1982; Mäkelä *et al*., 1996; Lu *et al*., 2016). Yet, for such a plant to make full use of its carbon investments in water uptake and

transport, it must nevertheless allow ψ_L to approach a safe lower limit at some time, and throughout the canopy – at which point biophysics and economics would constrain ψ_L from below and above, respectively, as described earlier. Second, real leaves need to maintain a safety margin between ψ_L and ψ_c, to prevent rapid excursions in evaporative demand or soil water potential from causing fatal excursions of ψ_L below ψ_c (Sperry, 2000; Delzon & Cochard, 2014). But that need also reflects a biophysical constraint. If stomata could respond instantly to the environment, transient excursions would be impossible and the safety margin would reduce to an infinitesimal sliver. Since finite stomatal response rates are biophysical constraints like ψ_c itself, the size of the safety margin is dictated by biophysical constraints (on stomatal kinetics) and environmental variables (the likelihood of dangerously rapid excursions in evaporative demand or soil water potential) (Meinzer *et al.*, 2017), and therefore does not represent freedom for leaf water potential to vary arbitrarily as needed to satisfy Eqn 19.

If ψ_L is not a truly free parameter, the only remaining parameter in Eqn 19 that the plant can control is K, which the plant can adjust via carbon partitioning. It follows that the optimal spatial distribution of water use (and by extension the total water use across the canopy) is defined by the optimal pattern of carbon partitioning. That is, canopy transpiration rate is an *outcome* of optimization, so it cannot be treated as a prior constraint in the optimization problem. The solution that arises from treating canopy transpiration as an imposed constant – that $\partial A/\partial E$ should be spatially invariant – is therefore invalid.

Why is it optimal for $\partial A/\partial E$ and $\partial A/\partial K$ to be smaller, and photosynthetic capacity per unit irradiance greater, in shaded leaves?

The argument presented earlier explains why the Lagrange multiplier approach is inappropriate for identifying the optimal spatial distribution of water loss in the canopy, but it does not explain why $\partial A/\partial E$ should vary in the specific manner predicted. A simple thought experiment can explain this result. First, it stands to reason that hydraulic conductance should be smaller in shaded modules than in sunlit modules, because the rates of photosynthesis and transpiration are smaller in shaded modules. For a given module leaf area, the only way to achieve smaller module K is by reducing carbon investment in the module's stem component, which determines stem hydraulic conductance (K_S). However, because stem carbon (C_S) earns diminishing returns in terms of module water use (that is, $\partial^2 E/\partial C_S^2 < 0$; Eqn S7 in Methods S8), reducing K_S leads to an increase in the marginal return on stem carbon ($\partial E/\partial C_S$). Optimal carbon partitioning requires the marginal sensitivity of carbon gain to stem carbon ($\partial A/\partial C_S$) to be invariant among modules (Buckley & Roberts, 2006b); to reconcile invariant $\partial A/\partial C_S$ with increasing $\partial E/\partial C_S$, $\partial A/\partial E$ must be smaller in shaded modules than in sunlit modules (because $\partial A/\partial C_S = (\partial A/\partial E)\cdot(\partial E/\partial C_S)$).

This reasoning also resolves the apparent contradiction between my results and those of Peltoniemi *et al.* (2012), who concluded that photosynthetic capacity and irradiance should remain proportional between shaded and sunlit leaves if both hydraulic conductance and nitrogen are distributed optimally. Peltoniemi *et al.* (2012) assumed that optimal distribution of hydraulic conductance is equivalent to invariance in $\partial A/\partial K$ ($= [\partial A/\partial E]\cdot[\partial E/\partial K] \approx [\partial A/\partial E]\cdot[\psi_{soil} - \psi_L]$); however, as discussed earlier and illustrated in Fig. 5, optimal carbon partitioning actually requires $\partial A/\partial K$ to vary between canopy modules. My simulations suggest that, in practice, differences in both $\partial A/\partial E$ and ψ_L contribute to satisfying this requirement. If ψ_L has less room to vary (e.g. because the risk curve is very steep; Eqn 18), then $\partial A/\partial E$ must differ more between modules, and vice versa (Fig. 5).

Other factors that commonly differ between shaded and sunlit modules, such as evaporative demand (Δw) and hydraulic pathlength (l), can magnify differences in $\partial K/\partial C_S$ and/or $\partial A/\partial K$, and thus also in photosynthetic capacity per unit irradiance. For example, if water must travel farther to reach sunlit leaves, then $\partial K/\partial C_S$ will be smaller for sunlit modules for a given K_S (Eqn S5 in Methods S2); invariance of $\partial A/\partial C_S$ then requires either even-larger $\partial A/\partial E$ or even-lower ψ_L in sunlit leaves. My results suggest that the relative importance of Δw and pathlength in driving variation in capacity per unit irradiance may vary widely with conditions (Figs 3, 4), consistent with a recent study (Bachofen *et al.*, 2020). Importantly, however, differences in evaporative demand and pathlength are not required to explain the general observation that shaded leaves have more N relative to their light environments: that pattern is optimal even if Δw and pathlength are identical between modules (Figs 3, 4).

Why does optimal carbon partitioning *not* lead to variation in $\partial A/\partial N$ within the canopy?

I found, as previously suggested (e.g. Field, 1983; Eqn 1), that it is optimal for the marginal carbon product of nitrogen, $\partial A/\partial N$, to be invariant in a canopy (if the goal function is carbon profit (P) rather than canopy photosynthesis, then it is $\partial P/\partial N$ that must be invariant; Fig. 5). Why does the argument developed earlier in relation to $\partial A/\partial E$ not apply to nitrogen? The reason is that nitrogen can, in principle, be partitioned arbitrarily between canopy modules. Although any given N partitioning may not be *economically* sensible – for example, building a high-N leaf in the shade would be uneconomical – there is no obvious *biophysical* constraint coupling C and N partitioning among modules, as there is for water. The total supply of photosynthetic N for the canopy can therefore be treated as a prior constraint for identifying optimal N distributions, so Eqn 1 remains valid.

Implications for predicting and interpreting canopy profiles of gas exchange parameters

I found that it is generally optimal for photosynthetic capacity per unit irradiance to be greater in shaded leaves than in sunlit leaves. This has two significant implications. First, it suggests that optimal N distribution does not generally make leaf-scale models of photosynthesis scale-invariant (Farquhar, 1989). The notion that optimization implies scale-invariance is the basis for 'big-leaf' scaling of photosynthesis from leaves to canopies. However, the nonoptimality of scale-invariance has few if any practical implications for

modeling, because it has long been understood that actual N profiles diverge from those assumed in big-leaf models, and efficient and accurate scaling procedures exist that can accommodate empirical profiles of N (e.g. de Pury & Farquhar, 1997). Second, observed canopy profiles of photosynthetic capacity are not necessarily suboptimal, as has long been suspected. Recent work has suggested that genetic variation in these profiles could be used to improve canopy carbon gain in crops (Townsend *et al.*, 2018; Yin *et al.*, 2019; Salter *et al.*, 2020). My results do not necessarily contradict that idea, but they do suggest that 'optimal' profiles are not necessarily those in which the capacity and irradiance ratios remain proportional through the canopy. More generally, by partially reconciling optimization theory with one class of observations that have long been thought to contradict the theory, my results support the use of optimization to predict plant form and function.

My results still diverge from observations for low irradiance ratios (i.e. very shaded leaves; Fig. 7). The reason for that divergence is unclear, and may involve processes that were omitted from my analysis. In particular, this study's focus on C and N partitioning at long timescales leaves open important questions involving shorter-timescale processes, such as diurnal stomatal movements and sunflecks. The impact of such processes on the economic tradeoffs underlying my results is not obvious, and cannot be rigorously deduced without a more detailed analysis. Some theoretical work (Buckley *et al.*, 2013) suggests that accounting for sunflecks introduces a large amount of scatter in the optimal relationship between irradiance and photosynthetic capacity, but does not systematically alter the overall trend. To account for short-term processes by adding a temporal dimension to this analysis would dramatically increase the number of optimized parameters, quickly rendering the problem intractable with the current approach. A novel approach may thus be needed to extend these results to include finer-scale processes.

Conclusions

Optimization of carbon partitioning in a whole plant model predicts that it is optimal for photosynthetic capacity per unit irradiance to be greater in more shaded canopy modules than in more sunlit modules, thus helping to reconcile optimization theory with observations. This result holds in the absence of differences in evaporative demand or hydraulic pathlength between modules. Spatial invariance of the marginal carbon revenue of nitrogen, $\partial A/\partial N$, is optimal as previously noted, but the marginal carbon revenues of both water ($\partial A/\partial E$) and hydraulic conductance ($\partial A/\partial K$) should vary through the canopy in the optimum.

Acknowledgements

I thank the National Science Foundation (Awards #1557906 and #1951244) and the USDA National Institute of Food and Agriculture (Hatch project 1016439 and Award no. 2020-67013-30913) for support.

ORCID

Thomas N. Buckley https://orcid.org/0000-0001-7610-7136

References

Ambrose AR, Baxter WL, Wong CS, Burgess SS, Williams CB, Næsborg RR, Koch GW, Dawson TE. 2016. Hydraulic constraints modify optimal photosynthetic profiles in giant sequoia trees. *Oecologia* **182**: 713–730.

Amthor JS. 1994. Scaling CO_2-photosynthesis relationships from the leaf to the canopy. *Photosynthesis Research* **39**: 321–350.

Bachofen C, D'Odorico P, Buchmann N. 2020. Light and VPD gradients drive foliar nitrogen partitioning and photosynthesis in the canopy of European beech and silver fir. *Oecologia* **192**: 323–339.

Bond BJ, Farnsworth BT, Coulombe RA, Winner WE. 1999. Foliage physiology and biochemistry in response to light gradients in conifers with varying shade tolerance. *Oecologia* **120**: 183–192.

Buckley TN. 2019. How do stomata respond to water status? *New Phytologist* **224**: 21–36.

Buckley TN, Cescatti A, Farquhar GD. 2013. What does optimisation theory actually predict about crown profiles of photosynthetic capacity, when models incorporate greater realism? *Plant, Cell & Environment* **36**: 1547–1563.

Buckley TN, Martorell S, Diaz-Espejo A, Tomàs M, Medrano H. 2014. Is stomatal conductance optimized over both time and space in plant crowns? A field test in grapevine (*Vitis vinifera*). *Plant, Cell & Environment* **37**: 2707–2721.

Buckley TN, Miller JM, Farquhar GD. 2002. The mathematics of linked optimisation for nitrogen and water use in a canopy. *Silva Fennica* **36**: 639–669.

Buckley TN, Roberts DW. 2006a. DESPOT, a process-based tree growth model that allocates carbon to maximize carbon gain. *Tree Physiology* **26**: 129–144.

Buckley TN, Roberts DW. 2006b. How should leaf area, sapwood area and stomatal conductance vary with tree height to maximise growth? *Tree Physiology* **26**: 145–157.

Centritto M, Loreto F, Chartzoulakis K. 2003. The use of low [CO_2] to estimate diffusional and non-diffusional limitations of photosynthetic capacity of salt-stressed olive saplings. *Plant, Cell & Environment* **26**: 585–594.

Chaves MM, Flexas J, Pinheiro C. 2009. Photosynthesis under drought and salt stress: regulation mechanisms from whole plant to cell. *Annals of Botany* **103**: 551–560.

Choat B, Jansen S, Brodribb TJ, Cochard H, Delzon S, Bhaskar R, Bucci SJ, Feild TS, Gleason SM, Hacke UG. 2012. Global convergence in the vulnerability of forests to drought. *Nature* **491**: 752.

Cowan IR. 1982. Water use and optimization of carbon assimilation. In: Lange OL, Nobel CB, Osmond CB, Ziegler H, eds. *Encyclopedia of plant physiology. 12B. Physiological plant ecology.* Berlin, Germany: Springer-Verlag, 589–630.

Cowan IR, Farquhar GD. 1977. Stomatal function in relation to leaf metabolism and environment. *Symposium of the Society for Experimental Biology* **31**: 471–505.

Delzon S, Cochard H. 2014. Recent advances in tree hydraulics highlight the ecological significance of the hydraulic safety margin. *New Phytologist* **203**: 355–358.

Delzon S, Sartore M, Burlett R, Dewar R, Loustau D. 2004. Hydraulic responses to height growth in maritime pine trees. *Plant, Cell & Environment* **27**: 1077–1087.

Downton W, Loveys B, Grant W. 1988. Non-uniform stomatal closure induced by water stress causes putative non-stomatal inhibition of photosynthesis. *New Phytologist* **110**: 503–509.

Eller CB, Rowland L, Mencuccini M, Rosas T, Williams K, Harper A, Medlyn BE, Wagner Y, Klein T, Teodoro GS *et al.* 2020. Stomatal optimization based on xylem hydraulics (SOX) improves land surface model simulation of vegetation responses to climate. *New Phytologist* **226**: 1622–1637.

Evans JR. 1993. Photosynthetic acclimation and nitrogen partitioning within a lucerne canopy. I. Canopy characteristics. *Australian Journal of Plant Physiology* **20**: 55–67.

Evans JR. 1996. Developmental constraints on photosynthesis: effects of light and nutrition. In: Baker NR, ed. *Photosynthesis and the environment.* Dordrecht, the Netherlands: Springer, 281–304.

Farquhar GD. 1989. Models of integrated photosynthesis of cells and leaves. *Philosophical Transactions of the Royal Society of London, Series B* **323**: 357–367.

Farquhar GD, Buckley TN, Miller JM. 2002. Stomatal control in relation to leaf area and nitrogen content. *Silva Fennica* **36**: 625–637.

Farquhar GD, von Caemmerer S, Berry JA. 1980. A biochemical model of photosynthetic CO_2 assimilation in leaves of C_3 species. *Planta* **149**: 78–90.

Field C. 1983. Allocating leaf nitrogen for the maximization of carbon gain: leaf age as a control on the allocation program. *Oecologia* **56**: 341–347.

Frak E, Le Roux X, Millard P, Adam B, Dreyer E, Escuit C, Sinoquet H, Vandame M, Varlet-Grancher C. 2002. Spatial distribution of leaf nitrogen and photosynthetic capacity within the foliage of individual trees: disentangling the effects of local light quality, leaf irradiance, and transpiration. *Journal of Experimental Botany* **53**: 2207–2216.

Friend AD. 2001. Modelling canopy CO_2 fluxes: are 'big-leaf' simplifications justified? *Global Ecology and Biogeography* **10**: 603–619.

Hikosaka K, Anten NP, Borjigidai A, Kamiyama C, Sakai H, Hasegawa T, Oikawa S, Iio A, Watanabe M, Koike T. 2016. A meta-analysis of leaf nitrogen distribution within plant canopies. *Annals of Botany* **118**: 239–247.

Hirose T, Werger MJA. 1987. Maximizing daily canopy photosynthesis with respect to the leaf nitrogen allocation pattern in the canopy. *Oecologia* **72**: 520–526.

Hirose T, Werger M, Pons T, Van Rheenen J. 1988. Canopy structure and leaf nitrogen distribution in a stand of *Lysimachia vulgaris* L. as influenced by stand density. *Oecologia* **77**: 145–150.

Hirose T, Werger MJA. 1994. Photosynthetic capacity and nitrogen partitioning among species in the canopy of a herbaceous plant community. *Oecologia* **100**: 203–212.

Hirose T, Werger MJ. 1995. Canopy structure and photon flux partitioning among species in a herbaceous plant community. *Ecology* **76**: 466–474.

Hollinger DY. 1996. Optimality and nitrogen allocation in a tree canopy. *Tree Physiology* **16**: 627–634.

Iio A, Fukasawa H, Nose Y, Kato S, Kakubari Y. 2005. Vertical, horizontal and azimuthal variations in leaf photosynthetic characteristics within a *Fagus crenata* crown in relation to light acclimation. *Tree Physiology* **25**: 533–544.

Kaiser W. 1987. Effects of water deficit on photosynthetic capacity. *Physiologia Plantarum* **71**: 142–149.

Koch GW, Sillett SC, Jennings GM, Davis SD. 2004. The limits to tree height. *Nature* **42**: 851–854.

Kull O. 2002. Acclimation of photosynthesis in canopies: models and limitations. *Oecologia* **133**: 267–279.

Lawlor DW, Tezara W. 2009. Causes of decreased photosynthetic rate and metabolic capacity in water-deficient leaf cells: a critical evaluation of mechanisms and integration of processes. *Annals of Botany* **103**: 561–579.

Lloyd J, Patino S, Paiva RQ, Nadrdoto GB, Quesada CA, Santos AJB, Baker TR, Brand WA, Hilke I, Gielmann H *et al.* 2010. Optimisation of photosynthetic carbon gain and within-canopy gradients of associated foliar traits for Amazon forest trees. *Biogeosciences* **7**: 1833–1859.

Louarn G, Frak E, Zaka S, Prieto J, Lebon E. 2015. An empirical model that uses light attenuation and plant nitrogen status to predict within-canopy nitrogen distribution and upscale photosynthesis from leaf to whole canopy. *AoB Plants* **7**: plv116.

Lu Y, Duursma RA, Medlyn BE. 2016. Optimal stomatal behaviour under stochastic rainfall. *Journal of Theoretical Biology* **394**: 160–171.

Mäkelä A, Berninger F, Hari P. 1996. Optimal control of gas exchange during drought: theoretical analysis. *Annals of Botany* **77**: 461–467.

Makino A, Sato T, Nakano H, Mae T. 1997. Leaf photosynthesis, plant growth and nitrogen allocation in rice under difference irradiances. *Planta* **203**: 390–398.

McCulloh KA, Domec J-C, Johnson DM, Smith DD, Meinzer FC. 2019. A dynamic yet vulnerable pipeline: Integration and coordination of hydraulic traits across whole plants. *Plant, Cell & Environment* **42**: 2789–2807.

Meinzer FC, Smith DD, Woodruff DR, Marias DE, McCulloh KA, Howard AR, Magedman AL. 2017. Stomatal kinetics and photosynthetic gas exchange along a continuum of isohydric to anisohydric regulation of plant water status. *Plant, Cell & Environment* **40**: 1618–1628.

Niinemets U. 2012. Optimization of foliage photosynthetic capacity in tree canopies: towards identifying missing constraints. *Tree Physiology* **32**: 505–509.

Niinemets Ü, Keenan TF, Hallik L. 2015. A worldwide analysis of within-canopy variations in leaf structural, chemical and physiological traits across plant functional types. *New Phytologist* **205**: 973–993.

Peltoniemi MS, Duursma RA, Medlyn BE. 2012. Co-optimal distribution of leaf nitrogen and hydraulic conductance in plant canopies. *Tree Physiology* **32**: 510–519.

de Pury DGG, Farquhar GD. 1997. Simple scaling of photosynthesis from leaves to canopies without the errors of big-leaf models. *Plant, Cell & Environment* **20**: 537–557.

Quick W, Chaves M, Wendler R, David M, Rodrigues M, Passaharinho J, Pereira J, Adcock M, Leegood R, Stitt M. 1992. The effect of water stress on photosynthetic carbon metabolism in four species grown under field conditions. *Plant, Cell & Environment* **15**: 25–35.

Rohatgi A. 2020. *WebPlotDigitizer*. California, USA: Pacifica.

Ryan MG, Yoder BJ. 1997. Hydraulic limits to tree height and tree growth. *BioScience* **47**: 235–242.

Salter WT, Merchant A, Trethowan RM, Richards RA, Buckley TN. 2020. Wide variation in the suboptimal distribution of photosynthetic capacity in relation to light across genotypes of wheat. *AoB PLANTS* **12**: plaa039.

Sands PJ. 1995. Modelling canopy production. I. Optimal distribution of photosynthetic resources. *Australian Journal of Plant Physiology* **22**: 593–601.

Sharkey TD, Seemann JR. 1989. Mild water stress effects on carbon-reduction-cycle intermediates, ribulose bisphosphate carboxylase activity, and spatial homogeneity of photosynthesis in intact leaves. *Plant Physiology* **89**: 1060–1065.

Sperry JS. 2000. Hydraulic constraints on gas exchange. *Agricultural and Forest Meteorology* **104**: 13–23.

Sperry JS, Venturas MD, Anderegg WR, Mencuccini M, Mackay DS, Wang Y, Love DM. 2017. Predicting stomatal responses to the environment from the optimization of photosynthetic gain and hydraulic cost. *Plant, Cell & Environment* **40**: 816–830.

Townsend AJ, Retkute R, Chinnathambi K, Randall JW, Foulkes J, Carmo-Silva E, Murchie EH. 2018. Suboptimal acclimation of photosynthesis to light in wheat canopies. *Plant Physiology* **176**: 1233–1246.

Tyree MT, Sperry JS. 1988. Do woody plants operate near the point of catastrphic xylem dysfunction caused by dynamic water stress? Answers from a model. *Plant Physiology* **88**: 574–580.

Tyree MT, Sperry JS. 1989. Vulnerability of xylem to cavitation and embolism. *Annual Review of Plant Physiology and Molecular Biology* **40**: 19–38.

Wolf A, Anderegg WR, Pacala SW. 2016. Optimal stomatal behavior with competition for water and risk of hydraulic impairment. *Proceedings of the National Academy of Sciences, USA* **113**: E7222–E7230.

World Meteorological Organization. 2008. *Guide to Meteorological Instruments and Methods of Observation*. Geneva, Switzerland: WMO.

Yin L, Xu H, Dong S, Chu J, Dai X, He M. 2019. Optimised nitrogen allocation favours improvement in canopy photosynthetic nitrogen-use efficiency: Evidence from late-sown winter wheat. *Environmental and Experimental Botany* **159**: 75–86.A1

Appendix A1

Photosynthesis model

The net photosynthesis rate for a given module ($A_{(m)}$) is calculated from the Farquhar, von Caemmerer and Berry (FvCB) model (Farquhar *et al.*, 1980), assuming that photosynthesis can be limited either by ribulose 1,5-bisphosphate (RuBP) carboxylation ($A_{(m)} = A_{V(m)}$) or by RuBP regeneration ($A_{(m)} = A_{J(m)}$):

$$A_{V(m)} = V_{M(m)} \frac{c_{i(m)} - \Gamma_*}{c_{i(m)} + K'} - R_{d(m)}, \qquad \text{Eqn A1}$$

$$A_{J(m)} = J_{(m)} \frac{c_{i(m)} - \Gamma_*}{c_{i(m)} + 2\Gamma_*} - R_{d(m)}, \qquad \text{Eqn A2}$$

where $V_{M(m)}$ is carboxylation capacity, $J_{(m)}$ is potential electron transport rate, $c_{i(m)}$ is intercellular CO_2 concentration, Γ_* is photorespiratory CO_2 compensation point, K' is the effective Michaelis constant for carboxylation, and $R_{d(m)}$ is the rate of

nonphotorespiratory CO_2 release in the light. J is computed as the hyperbolic minimum of the maximum potential electron transport rate ($J_{M(m)}$) and the product of effective quantum yield of electrons (ϕ) and incident PPFD ($i_{(m)}$):

$$\theta_J J_{(m)}^2 - J\left(J_{M(m)} + \phi i_{(m)}\right) + J_{M(m)}\phi i_{(m)} = 0, \qquad \text{Eqn A3}$$

where θ_J is a dimensionless convexity parameter ≤ 1. ϕ is given by $\phi = 0.5 \cdot \alpha\ \phi_{PSIImax}$, where $\phi_{PSIImax}$ is the maximum quantum yield of photosystem II, and α is leaf absorptance to photosynthetically active radiation, which depends on Chl content (mmol m^{-2}) (Evans, 1996):

$$\alpha = \frac{\text{Chl}}{\text{Chl} + 0.076}. \qquad \text{Eqn A4}$$

Chl depends on N invested in light capture ($N_{C(m)}$) and electron transport ($N_{J(m)}$) as (Buckley *et al.*, 2013):

$$\text{Chl} = \chi_{cj} N_{J(m)} + \chi_c N_{C(m)}, \qquad \text{Eqn A5}$$

$V_{M(m)}$ and $J_{M(m)}$ depend on module-wise N pools for Rubisco ($N_{V(m)}$) and electron transport:

$$V_{M25(m)} = \chi_V N_{V(m)}, \qquad \text{Eqn A6}$$

$$J_{M25(m)} = \chi_J N_{J(m)}, \qquad \text{Eqn A7}$$

where χ_V and χ_J are fixed parameters and the subscripts '25' indicate values at 25°C. The parameters V_M, J_M, Γ_*, K', $\phi_{PSIImax}$, θ_J and R_d all depend directly on temperature (see Supporting information Methods S9). I assumed that $R_{d(m)}$ is proportional to $V_{M(m)}$ at 25°C, such that $R_{d25(m)} = 0.0089 \cdot V_{M25(m)}$ (de Pury & Farquhar, 1997). $N_{J(m)}$, $N_{V(m)}$ and $N_{C(m)}$ are determined by optimal partitioning of the total available N (N_{TOTAL}, Eqn 16 in the main text) between modules, and among these three functional pools within each module. Intercellular CO_2 concentration is determined by the balance between CO_2 demand by the mesophyll (Eqns A1 and A2) and diffusional supply through the stomata:

$$A_{(m)} = \frac{g_{sw(m)} g_{bw(m)}}{1.6 g_{bw(m)} + 1.37 g_{sw(m)}}\left(c_a - c_{i(m)}\right), \qquad \text{Eqn A8}$$

where c_a is ambient CO_2 concentration, and g_{sw} and g_{bw} are stomatal and boundary layer conductances to water vapor, respectively (Eqn A8 ignores mesophyll conductance). Combining Eqn A8 with either Eqns A1 or A2 produces a quadratic expression for $c_{i(m)}$, whose solution for c_i can be applied to Eqns A1 or A2 to determine $A_{V(m)}$ or $A_{J(m)}$, respectively. Assimilation rate is usually calculated as the simple minimum of $A_{V(m)}$ and $A_{J(m)}$; because that produces discontinuities in A, which can preclude unambiguous identification of optima, I 'smoothed' the transition between $A_{V(m)}$ and $A_{J(m)}$ by computing $A_{(m)}$ as the hyperbolic minimum of $A_{V(m)}$ and $A_{J(m)}$ with the dimensionless parameter θ_A to 0.999:

$$\theta_A A_{(m)}^2 - A\left(A_{V(m)} + A_{J(m)}\right) + A_{V(m)} A_{J(m)} = 0. \qquad \text{Eqn A9}$$

Supporting Information

Additional Supporting Information may be found online in the Supporting Information section at the end of the article.

Fig. S1 Distributions of profit from uniqueness validation analysis, demonstrating that the optimal solutions presented in the main text are unique and global solutions.

Fig. S2 Distributions of parameter values from uniqueness validation analysis, demonstrating that optimized parameters were essentially identical across solutions identified using randomized initial parameter estimates.

Fig. S3 Simulations with carbon gain rather than carbon profit as the goal, showing small differences in the relationships between capacity and irradiance ratios.

Fig. S4 Parameter sensitivity analysis, showing that variation in most parameter values had little effect on optimal capacity ratios at an intermediate irradiance ratio of 0.5.

Methods S1 Derivation of expressions for water use in each module.

Methods S2 Derivation of expressions for hydraulic conductances.

Methods S3 Derivation of expression for leaf temperature.

Methods S4 Description of numerical optimization routine and uniqueness validation.

Methods S5 R code implementing the model.

Methods S6 CSV file, used in the R code, containing input parameters.

Methods S7 Parameter estimation.

Methods S8 Response of water use to stem carbon investment, and comparison between modules.

Methods S9 Temperature dependencies of photosynthetic parameters.

Please note: Wiley Blackwell are not responsible for the content or functionality of any Supporting Information supplied by the authors. Any queries (other than missing material) should be directed to the *New Phytologist* Central Office.